Intelligence-Based Medicine 10 (2024) 100183

Contents lists available at ScienceDirect

Intelligence-Based Medicine

journal homepage: www.sciencedirect.com/journal/intelligence-based-medicine

# Temporal convolutional network on Raman shift for human osteoblast cells fingerprint Analysis[a,b,c]

Dario Morganti [a,b,1], Maria Giovanna Rizzo [b,1], Massimo Orazio Spata [c,*], Salvatore Guglielmino [b], Barbara Fazio [a], Sebastiano Battiato [c], Sabrina Conoci [a,b]

[a] CNR DSFTM-ME, URT LabSens Beyond Nano Messina, Viale F. S. d'Alcontres, 31 I, 98166, Messina, Italy
[b] Italy Dipartimento di Scienze chimiche, biologiche, farmaceutiche e ambientali University of Messina, Piazza Pugliatti, 1, 98122, Messina, Italy
[c] Dip. di Matematica e Informatica University of Catania Viale A. Doria 6, 95125, Catania, Italy

ARTICLE INFO

*Keywords:*
Deep learning
Raman spectroscopy
Human osteoblast cells

ABSTRACT

The physiological state and biological characteristics of cells play a crucial role in the study of several biological mechanisms that are at the basis of the life. Raman spectroscopy, a powerful non-destructive technique, has shown promise in providing unique molecular fingerprints of cells based on their vibrational states. However, the high-dimensional and noisy nature of Raman spectra poses significant challenges in precise cell classification. In this study, we present a novel deep learning algorithm tailored for human cells fingerprint assignment through Raman shift analysis. The proposed deep learning framework harnesses the power of Temporal Convolutional Networks (TCN) to efficiently extract and process Raman spectra information. Leveraging a dataset of labeled Raman spectra, the model is trained to learn discriminative features that capture the subtle differences in cell composition and molecular structures in differential states. Additionally, the proposed model enables real-time cell fingerprint prediction, making it highly applicable for high-throughput analysis in large-scale experiments. Experimental results demonstrate a peak accuracy of 99 %, showcasing the effectiveness and precision of the approach. Overall, the developed deep learning algorithm offers a robust and efficient solution for cell fingerprint assignment through Raman shift analysis, opening new avenues for advancements in physiological and biochemical studies.

## 1. Introduction

In recent years, the growing demand to know in more detail the composition and function of cells in a particular status has led to a great expansion of physiological studies. Accurate identification and classification of different cell types are prominent for understanding cellular behavior, disease stage, and drug development. Conventional methods for cell analysis, such. as fluorescence-based techniques, often involve invasive procedures and may interfere with cellular integrity, limiting their applicability in live cell studies. To overcome these limitations, Raman spectroscopy [1,2] has emerged as a promising non-invasive and label-free technique for cell analysis. Raman spectroscopy relies on the inelastic scattering of photons by molecules within a sample, resulting in characteristic Raman shifts that correspond to the vibrational modes of specific chemical bonds. This unique spectral information can be used as a "fingerprint" to differentiate different cell types and to study various cellular processes. However, the main challenge in Raman-based cell analysis lies

in extracting meaningful and informative features from the noisy Raman spectra [1]. With this respect Deep Learning Algorithms (DLA), combined with Raman investigation, can be an effective tool to overcome the limitation of the conventional methods for cellular processes investigation.

DLA have revolutionized various fields, including computer vision, natural language processing and medicine [3–5,6,7]. These algorithms have demonstrated remarkable performance in feature extraction and pattern recognition tasks [8–11]. The success of deep learning in various domains has inspired researchers to explore its potential in tackling challenges within spectroscopy and cell analysis [12]. This paper introduces a state-of-the-art deep learning algorithm specially designed for cell classification through Raman shift analysis. This topic has been explored in the literature in several applicative fields. In Ref. [13]

* Corresponding author.
*E-mail address:* massimo.spata@unict.it (M.O. Spata).
[1] author with equal contribution.

https://doi.org/10.1016/j.ibmed.2024.100183
Received 14 February 2024; Received in revised form 11 October 2024; Accepted 22 October 2024
Available online 24 October 2024

authors propose a practical convolutional neural network (CNN) model to distinguish between the Raman spectra of human and animal blood, demonstrating superior classification accuracy compared to PLSDA (Partial least squares-discriminant analysis) and SVM (Support Vector Machine). In Ref. [14], authors present a machine learning-based classification model designed to categorize extracellular vehicles (EVs) Raman spectra to identify those derived from tumors. The convolutional neural network (CNN) was trained using both preprocessed and raw Raman data. Authors compared the CNN's results with those obtained from the widely used principal component analysis (PCA) in spectroscopy. The proposed model achieved over 90 % accuracy in classifying EVs. The CNN model proved effective for directly classifying raw Raman data, achieving a minimum accuracy of 93 % without preprocessing. In Ref. [15], authors introduce Raman spectroscopy, to evaluate endoscopic disease severity based on the four-level Mayo subscore. The developed predictive model to detect colonic inflammation show a mean sensitivity of 78 % and a mean specificity of 93 % for the four Mayo endoscopic scores. In Ref. [16], authors introduce a nanoplasmonics biosensing chip (NBC) designed to facilitate antibody-free detection with simplified analysis for point-of-care testing (POCT). The authors developed a direct serological detection platform using this NBC and deep neural network (DNN) modeling to automatically identify liver cancer in minutes. The developed DNN classification model, trained on 1140 serum SERS spectra from both hepatocellular carcinoma (HCC) patients and healthy individuals, achieved 91 % identification accuracy on an external validation set of 100 spectra (50 HCC and 50 healthy). In Ref. [17], the authors introduced a new method called DeepCID (Deep Learning Component Identification), which uses deep learning for molecular identification through Raman spectroscopy. In this study, Convolutional Neural Network (CNN) models were developed to predict the presence of components in mixtures. Comparative analyses showed that DeepCID was highly effective at learning spectral features and identifying components in both simulated and real Raman spectral datasets of mixtures, resulting in higher accuracy and significantly lower false positive rates. Recent advances in pathogen detection and diagnosis of bacterial infections were discussed in Ref. [18], with focuses on the development of the SERS approaches and its applications in complex clinical settings. In Ref. [19] authors describe the basic principles of Raman Spectroscopy (RS), emphasizing the label-free SERS approach, highlights the latest advancements in SERS technology for detecting bacteria, viruses, and fungi in clinical environments. Surface-enhanced Raman spectroscopy (SERS) offers a highly effective method for detecting small molecular components with exceptional sensitivity and selectivity [20].

The goal of this work is to leverage the full potential of Raman spectroscopy and deep learning to enhance the accuracy, efficiency, and scalability of cell analysis, minimizing the need for laborious sample preparation and invasive labeling techniques that are used in the cells analysis applications, like histological analysis. The proposed deep learning framework builds upon the strength of Temporal Convolutional Networks (TCN) [21] in identifying spatial patterns and modeling temporal dependencies, effectively capturing the rich information present in Raman spectra. TCN are adept at recognizing local patterns in the spectral data, exploiting sequential dependencies, making it well-suited for analyzing time-dependent or sequential data, as for example in Refs. [5,22]. To train the model, a substantial dataset of labeled Raman spectra is essential. A dataset of 1384 Raman spectra of a specific human cell line (cell not treated and cell treated with peptide-phage) have been collected to enable the deep learning model to learn robust and generalizable features for accurate cell fingerprint analysis. Additionally, careful preprocessing and normalization techniques are employed to handle the inherent noise and fluctuations in Raman measurements, ensuring the model's resilience to experimental variations. Moreover, the model exhibits superior performance in real-time analysis, opening new avenues for high-throughput screening in large-scale experiments and clinical settings. One of the significant advantages of the proposed deep learning algorithm is its adaptability to different experimental setups and Raman instruments. The integration of Raman spectroscopy and deep learning represents a significant advancement in the field of cell biology [12]. The proposed deep learning algorithm not only enhances the accuracy and efficiency of cell classification but also expands the scope of Raman-based cell analysis to a wide range of applications, from fundamental research to clinical diagnostics and pharmaceutical development. By providing a non-invasive, label-free, and real-time solution for cell analysis, this cutting-edge approach promises to drive transformative discoveries and breakthroughs in cellular biology and medical research. In particular, the results here reported paves the way to the development of new method for histological analysis based on chemical fingerprint of cells instead of immune-based methodology. This will give a relevant improvement in the clinical diagnostic providing a clear cell identification in the pre- and post-surgical analyses.

The rest of the pages are organized as follows: section 2 introduces details at the proposed method, section 3 reports some experimental results, and section 4 exploits detailed results with discussions.

## 2. Proposed method

A Temporal Convolutional Network (TCN) is a type of deep learning architecture designed for sequential data processing. It employs one-dimensional convolutional layer to capture patterns and dependencies in temporal sequences efficiently, making it suitable for tasks such as time series forecasting, natural language processing, and audio analysis [23]. TCN are a powerful class of neural networks with several noteworthy features; TCN can efficiently process sequences in parallel, unlike recurrent neural networks (RNN) [24] that require sequential computation, making them faster for training and inference. It allows parallel computation on GPU in Nvidia video

Cards as in Ref. [25] or parallel CPU in virtual environments in cloud as in Ref. [26]. TCN often use dilated convolutions, allowing them to capture both short-term and long-term dependencies in the data effectively. This makes them suitable for tasks requiring context over varying time scales. TCN often employs causal convolutions, ensuring that predictions are not influenced by future inputs, which is essential for tasks like time series forecasting. Overall, TCN have become a valuable tool in the deep learning toolkit for modeling sequential data, offering advantages in terms of speed, parallelism, and modeling capabilities [21,23,26].

Causal convolution is calculated as:

$$y_i = \sum_{j=0}^{k-1} c_j x_{j-1} \tag{1}$$

where:

- $x_i$ – input tensor with shape (input size, 1)
- $y_i$ – output tensor with shape (num classes)
- $k$ – convolution kernel
- $c_j$ - convolution weights

The proposed TCN method, has been implemented the following causal convolution with convolution kernel k = 3 and padding = k −1 (Fig. 1).

To perform causal convolution, we incorporate padding (k-1) on the left side of the input tensor. Causal convolution embodies a straightforward logic; it gathers information and patterns that precede the current point in the data sequence. In fact, TCN models equipped with causal convolution layers excel at capturing dependencies that prove invaluable for predicting future values [21]. The practical application of these causal convolution layers is vividly illustrated in the pipeline properly showed in Fig. 2. To execute causal convolution, we employ classical 1-D convolution with padding and trim elements from the right

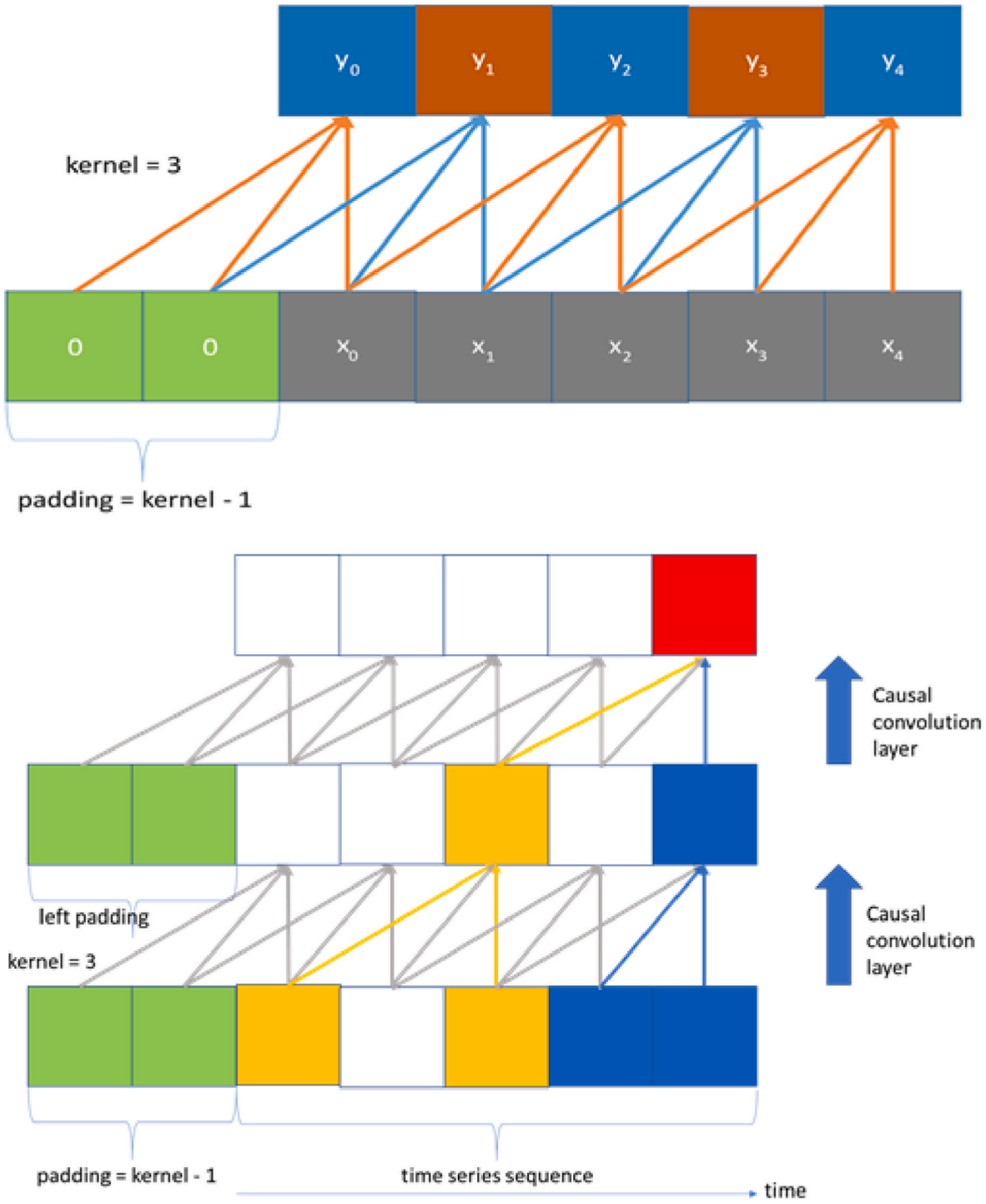


**Fig. 1.** Causal convolution with padding and kernel k = 3.

side. Employing the dilation technique within a causal convolutional layer enhances the coverage of the input time series and substantially reduces computational costs. In the TCN architecture, it is assumed that the sequence of causal convolutional layers has a dilation factor of $2^{i-1}$(*i = 0,.., n and n = number of hidden layers*). The overall configuration of our proposed TCN model architecture, is reported in Table 1. Utilizing ReLU as the activation function for TCN is recommended [26]. ReLU (Rectified Linear Unit) is preferred because it introduces non-linearity while being computationally efficient, helping to avoid issues like the vanishing gradient problem that can occur with other activation functions. This allows TCN to learn more effectively and converge faster during training. The stability of the TCN model was enhanced by switching to Binary Cross-Entropy for classification, which led to more reliable and accurate results. This adjustment specifically helped in improving the model's performance and robustness during training, lowering the learning rate for gradual learning, simplifying the architecture to reduce complexity, increasing the batch size for stable gradients, and raising the dropout rate to prevent overfitting. However, there are two more potential enhancement that can further boost the performance of a TCN: the dilated and causal convolution. In the context of our proposed TCN model architecture (as depicted in Fig. 2), we have applied a specific set of hyperparameters, which are detailed in Table I.

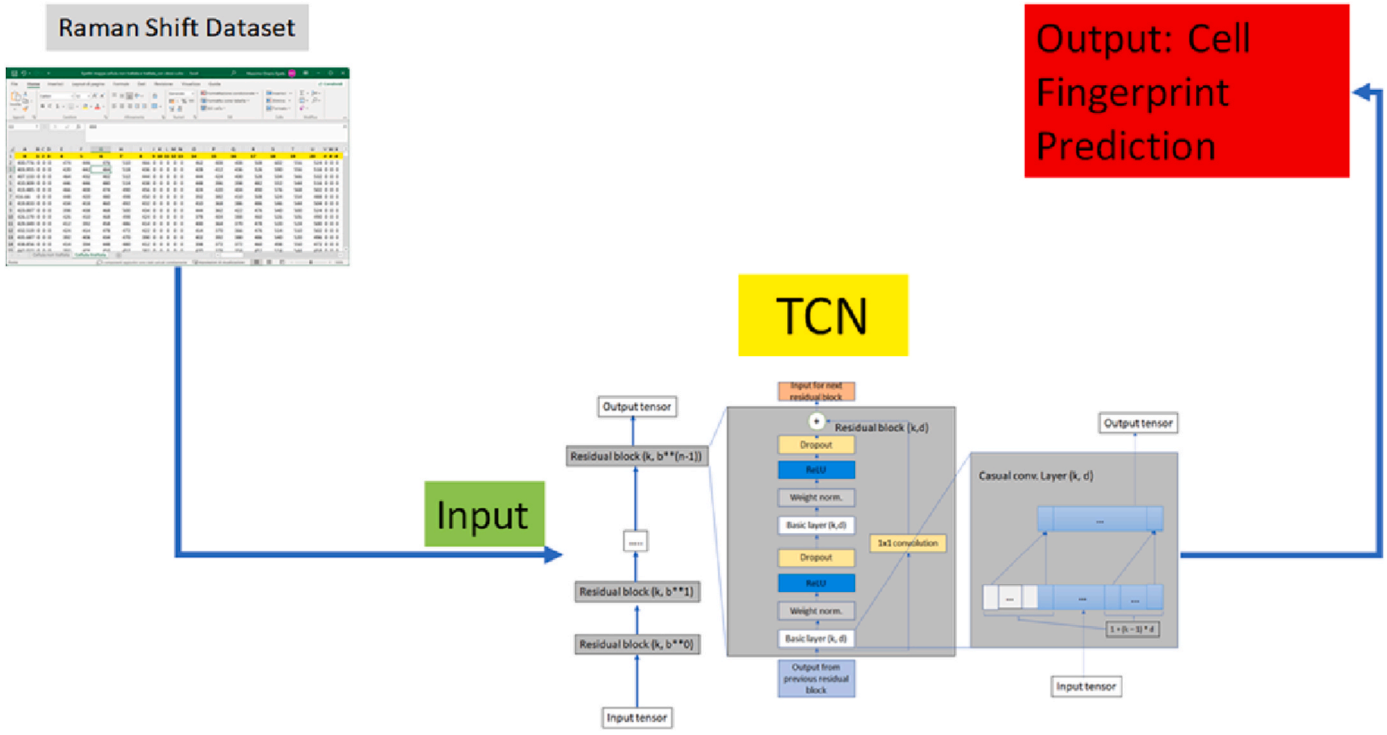


**Fig. 2.** Implemented Temporal Convolutional Network Model, and the proposed pipeline to extract cell classification (treated or not treated).

**Table 1**
TCN model setup.

| TCN Model Parameter | Values |
|---|---|
| Training set | 70 % |
| Validation set | 15 % |
| Test set | 15 % |
| Shuffle (random split) | True |
| Loss function | Binary_crossentropy |
| Optimizer | Adam |
| Learning rate | 0.00001 |
| Epochs | 100 |
| Input size | 121 |
| Hidden layers | 3 |
| Batch size | 256 |
| Num classes (output) | 1 |
| Kernel size | 3 |
| Dropout | 0.2 |

3. Data collection and measurement.

### 2.1. Cell culture

Human foetal osteoblast cell line (hFOB) 1.19 were obtained from the American Type Cul-ture Collection (ATCC, Manassas, VA, United States). hFOB 1.19 were cultured in 1:1 mixture of Ham's F12 Medium – Dulbecco's Modified Eagle's Medium (Merk Life Science S.r.l., Milan, Italy), supplemented with 2.5 mM L-glutamine (Merk Life Science S.r.l., Milan, Italy), 10 % Fetal Bovine Serum (FBS, Merk Life Science S.r.l., Milan, Italy) and 1 % penicillin/streptomycin/amphotericin (Merk Life Science S.r.l., Milan, Italy) and incubated in a humidified atmosphere containing 5 % $CO_2$ at 37 °C [27]. The medium was replaced twice a week and cells were split at about 80 % of confluence.

#### 2.1.1. Sample preparation

hFOB cells were collected after reaching 70 % with trypsin-EDTA solution. The pellet has been resuspended in culture medium and transferred onto $CaF_2$ slides, previously cleaned with a mixture of water and ethanol, at a concentration of 60000 cells per milliliter. We have been chosen $CaF_2$ slides as substrate that, for its optical features is suitable for spectroscopical investigation avoiding any spurious fluorescence signals coming from the support, which could significantly interfere with the Raman signals of the cells. The pellet has been resuspended in culture medium containing the peptide-phage suspension at $10^{11}$ TU/mL (TU = transducing unit). The peptide-phage, selected by phage display technology [28], exposed the peptide QRRAGPVPP that is mimotope of the growth factors and proteins involved in bone development. Untreated cells have been used as a control. In order to obtain hFOB cells in a prolonged growth state, the medium was discarded after 72 h of incubation. Then we have been washed the cells with phosphate buffered saline (PBS) without Ca and Mg and then fixed with 4 % formalin for 20 min. The sample has been finally washed in ultrapure water in order to perform Raman spectroscopy measurements.

### 2.2. Raman measurements

Raman measurements of the hFOB cell line were performed by using a $1 \times 1$ $cm^2$ of a $CaF_2$ commercial slide as a support substrate. Raman spectra were acquired focusing 1 μW of the 473 nm laser line (solid-state COBOLT) by a 100X objective (N.A. 0.9) mounted on an Olympus microscope. The backscattered Raman signals were captured over 40 s and collected using a Horiba iHR550 Spectrometer, equipped with a 600 lines/mm diffraction grating and coupled to a CCD detector (Syncerity Horiba). To acquire signals at regular intervals and spatial paths, the spectra were collected in the mapping mode of the Horiba software. The map was optimized to encompass the target cell, in order to facilitate the analysis of all cellular components, ranging from the nucleus to the outside of the cell. Within each map, we obtained 121 spectra, corresponding to an 11x11 point matrix.

## 3. Results

All methods have been implemented on a Python environment on a

PC with Intel(R) Core(TM) i7 CPU, 16 GB memory and NVIDIA RTX 2050 GPU. The dataset has been split in training (70 % of the total dataset), validation (15 %) and test (15 %) subsets and processed during training and evaluation of the TCN model. This ratio provides a balanced approach, offering enough data for training while reserving a sufficient portion for validation and testing. This 70/30 split is commonly used to ensure that the model can generalize well to new data, without overfitting, while still allowing for effective evaluation. Using other ratios like 6:2:2 or 8:2 might either reduce the data available for testing/validation or leave too little for training, potentially impacting model performance. Finally, TCN return the cell fingerprint.

The implemented pipeline for the TCN model includes the following steps:

- *Data preprocessing*: This step involves preparing the dataset for use with the TCN model. This may include cleaning and formatting the data, as well as splitting it into training, validation, and test sets.
- *Building the model*: This step involves designing and instantiating the TCN model. This may include specifying the number of layers, the number of filters, the kernel size, and the type of activation function to use.
- *Training the model*: This step involves using the training data to train the model. The model is typically trained using a variant of stochastic gradient descent (SGD) algorithm.
- *Evaluating the model*: This step involves using the validation and test data to evaluate the performance of the model. This may include metrics such as accuracy, precision, and MSE loss score, plotting the prediction and target data, verifying that it correctly calculates the cell fingerprint.
- *Deployment*: After the model has been trained and fine-tuned, it can be deployed in a production environment.

As loss function in the training, test and validation phase, has been exploited the Binary Cross Entropy function which measures the difference between predicted probabilities and actual binary outcomes for classification tasks. After 100 epochs, results shows that training and validation MSE and MAE converge to 0 as is showed in Fig. 4. It looks as though the line plot for the training set is dropping to converge with the line for the validation set. It means that prediction and target converge with a minimum loss error.

In Fig. 5 has been measured inference which refers to the process of using a trained model to make predictions or draw conclusions on new, unseen data. Once a deep learning model is trained on a labeled dataset, it learns patterns, relationships, and representations from the training data, enabling make predictions on previously unseen data points during the inference phase. Data showed in Fig. 5 shows a good inference plot with a clear overlap between the predicted and target curves, indicating accurate predictions and a strong alignment between model outputs and actual data. In particular Fig. 5 shows the accuracy of the applied TCN model, with a peak accuracy of 99 % and the TCN inference on a single subset of 25 points of a Raman spectra between not treated cell and all dataset (treated cell and not treated cell).

In Table 2 it has been reported a benchmark of the presented architecture model with other models for the same dataset with treated and untreated cells. Experimental results demonstrate Temporal Convolutional Networks (TCN) offer a captivating twist in the realm of sequence modeling, blending the ingenuity of dilated and causal convolutions. Imagine TCN as master detectives of neural networks, adept at deducing

Patterns and dependencies across time without missing a beat. Dilated convolutions in TCN widen the field of view over the input sequence exponentially, zooming in on crucial details. This unique feature allows TCN to capture long-range dependencies efficiently, ideal for tasks where context across extensive temporal spans matter. Enter causal convolutions, ensuring that each output at time step $t$ depends only on past or current inputs, but not future ones a crucial twist in sequence tasks where predicting the future isn't straightforward. In essence, TCN excel in processing sequential data with long-term dependencies, maintaining order and coherence through causality, and elegantly handling variable length inputs with their flexible architecture. For tasks demanding a keen sense of temporal nuances, TCN step up as the go-to solution, unraveling patterns with precision and reliability. In essence, TCN excel in processing sequential data with long-term dependencies, maintain order and coherence through causality, and can elegantly handle variable-length inputs with their flexible architecture. So, when faced with tasks demanding a keen sense of temporal nuances, TCN step up as the detective of choice unraveling patterns with the precision and reliability.

## 4. Discussion

We developed a computational tool capable of determining and predicting differences between two cells typology by the analysis of their relative Raman. To this aim, hFOB cells were analyzed by Raman spectroscopy as showed in Fig. 3. Here, the Raman spectra of hFOB 1.19 cells bare (a) and treated with phages (b) are reported. In every spectrum, 3a and 3b discern the vibrational contributions of the cellular protein pattern, even without the subtraction of the fluorescence background. In particular, we can distinguish the peak related to the phenylalanine aromatic ring symmetric stretching (breathing mode) centered at 1005 $cm^{-1}$, the band of the —$CH_2$ deformations at 1450 $cm^{-1}$ and the bands of amide I at 1660 $cm^{-1}$ [29]. The most intense peak at 2936 $cm^{-1}$ is ascribed to the different vibration modes of the C—H groups. Finally, the band between 3200 and 3500 $cm^{-1}$ is attributable to

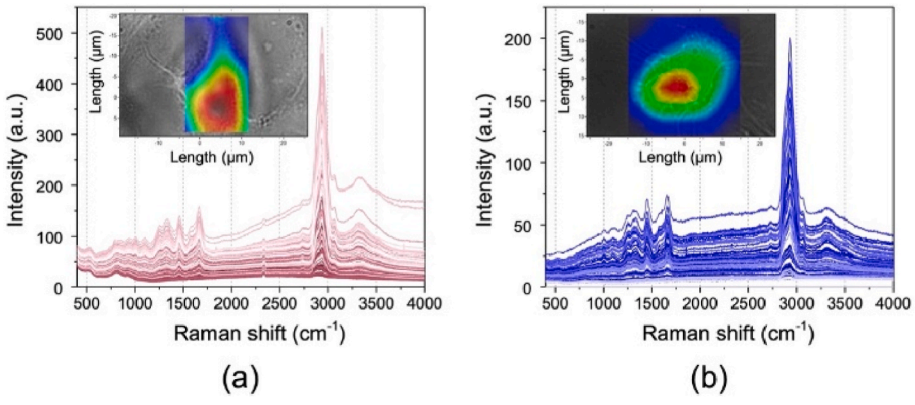


**Fig. 3.** Raman spectra acquired in mapping mode on untreated (a) and phage-treated (b) hFOB cells. The images of the target cells are shown in the insets; the area of the cell analyzed is highlighted by the RGB intensity map.

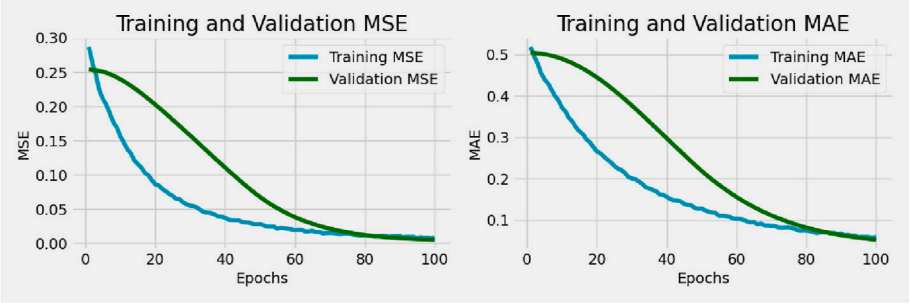


**Fig. 4.** MSE, MAE, Loss for training and validation for 100 epochs.

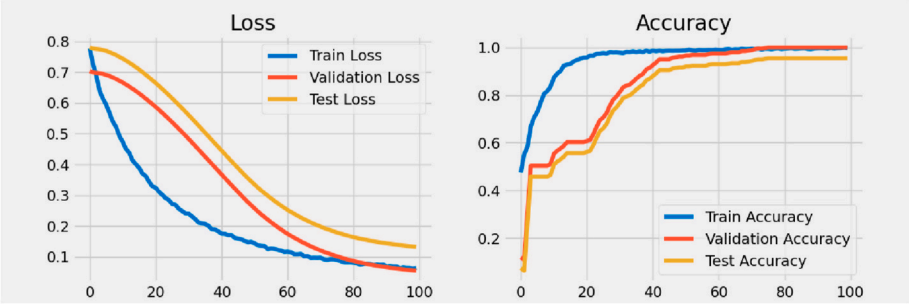


**Fig. 5.** Loss and Accuracy of the TCN model. The ground truth (target) is not treated cell dataset and prediction is calculated on all dataset with treated and not treated cell.

**Table 2**
Model comparation benchmark on the same input dataset of treated and untreated cells.

| Model | Accuracy | AUC | Recall | Prec. | F1 |
|---|---|---|---|---|---|
| TCN | 0.92 | 0.9 | 0.9 | 0.9 | 0.9 |
| MLP | 0.5 | 0.49 | 1 | 0.5 | 0.66 |
| Extra Trees | 0.5 | 0.5 | 1 | 0.5 | 0.66 |
| SVM | 0.49 | 0.5 | 0.1 | 0.04 | 0.06 |
| Log. Regr. | 0.49 | 0.5 | 0.7 | 0.34 | 0.46 |
| K Neighbors | 0.49 | 0.5 | 0.3 | 0.14 | 0.19 |
| Naïve Bayes | 0.49 | 0.5 | 0.3 | 0.14 | 0.19 |
| Decis. Tree | 0.49 | 0.5 | 0.3 | 0.14 | 0.19 |
| Rand. Forest | 0.49 | 0.5 | 0.3 | 0.14 | 0.19 |
| Ada Boost | 0.49 | 0.5 | 0.3 | 0.14 | 0.19 |
| LGBM | 0.49 | 0.5 | 0.3 | 0.14 | 0.19 |
| Ridge | 0.49 | 0.5 | 0.3 | 0.14 | 0.19 |
| QDA | 0.49 | 0.35 | 0.7 | 0.34 | 0.46 |
| LDA | 0.49 | 0.5 | 0.7 | 0.34 | 0.46 |

O—H stretching, typical of targets composed by an aqueous matrix. The insets within the graphs display images of the examined cells. The RGB map overlaid on these images effectively emphasizes the variations in Raman intensity across different regions of the cell within the frequency shift range of 800–1800 $cm^{-1}$. The regions in blue correspond to low Raman signal intensity, whereas the red regions exhibit high Raman signal intensity. It's evident that the red regions are primarily localized within the cell nucleus areas, which contain the highest concentration of proteins and genetic material (DNA, RNA, and nucleotides, in general). Therefore, even if the spectra reported in 3a and 3b figures could appear very similar, the analytical methods here reported is able to discern the right difference to be distinguished in terms of spectroscopical features. Therefore, it can be used for future further investigations.

## 5. Conclusions and future works

In this study, we have presented a novel deep learning algorithm for cell fingerprint analysis through Raman spectroscopy. The proposed approach leverages the power of convolutional neural networks (CNNs) and recurrent neural networks (RNNs) to extract and process Raman spectra information efficiently. Our findings demonstrate that the deep learning model achieves superior performance in accurately prediction of diverse cell types based on their Raman fingerprints. The results from our extensive evaluations indicate that the model's predictions align well with the ground truth data, with a significant overlap between the predicted and target curves in the inference plot. This overlap serves as a compelling indicator of the model's capability and ability to handle various experimental conditions, ultimately enhancing the utility of Raman spectroscopy for cell analysis. One of the significant strengths of our approach is its adaptability to different experimental setups and Raman instruments. The introduction of a transfer learning strategy enables the model to maintain high accuracy when applied to datasets acquired from different instruments or laboratories. This transfer learning approach reduces the need for extensive data labeling and collection, making the algorithm more cost-effective and widely applicable. This represents a preliminary study for future development in the field of chemical histology. Actually, despite the promising results achieved in this study, there are several avenues for further improvement and future research. Investigating more advanced transfer learning techniques, such as domain adaptation and fine-tuning, may lead to even better model performance across different Raman instruments and experimental conditions. Exploring the integration of multi-modal data, such as incorporating fluorescence or hyperspectral imaging alongside Raman spectra, could provide complementary information, potentially leading to more comprehensive and accurate cell classification. Expanding the size and diversity of the training dataset can further boost the model's generalization capacity and improve its performance on rare or less-studied cell types. In conclusion, the presented deep learning algorithm represents a significant advancement in the field of cell fingerprint assignment through Raman shift analysis. By addressing the outlined future research directions, this work opens new avenues for unlocking the full potential of Raman spectroscopy in advancing biochemical and physiological studies, paving the way for future development of new approach for cells histology based on chemical data

(chemical group vibrations).

## CRediT authorship contribution statement

**Dario Morganti:** Writing – review & editing, Writing – original draft, Data curation, Conceptualization. **Maria Giovanna Rizzo:** Writing – review & editing, Writing – original draft, Data curation, Conceptualization. **Massimo Orazio Spata:** Writing – review & editing, Writing – original draft, Validation, Software, Methodology, Formal analysis, Data curation, Conceptualization. **Salvatore Guglielmino:** Methodology, Investigation, Data curation, Conceptualization. **Barbara Fazio:** Writing – review & editing, Writing – original draft, Methodology, Formal analysis, Data curation, Conceptualization. **Sebastiano Battiato:** Writing – review & editing, Writing – original draft, Supervision, Formal analysis, Data curation, Conceptualization. **Sabrina Conoci:** Writing – review & editing, Writing – original draft, Validation, Supervision, Project administration, Methodology, Investigation, Formal analysis, Data curation, Conceptualization.

## Declaration of competing interest

The authors declare that they have no known competing financial interests or personal relationships that could have appeared to influence the work reported in this paper.

## References


[1] Jenkins Nia C, Ehrlich Katjana, Kufcsák András, Yerolatsitis Stephanos, Fernandes Susan, Young Irene, Hamilton Katie, Wood Harry AC, Quinn Tom, Young Vikki, Akram Ahsan R, Stone James M, Thomson Robert R, Finlayson Keith, Dhaliwal Kevin. Sohan seth: computational fluorescence suppression in shifted excitation Raman spectroscopy. IEEE Trans Biomed Eng 2023;70(8):2374–83.

[2] Dodo Kosuke, Fujita Katsumasa, Sodeoka Mikiko. Raman spectroscopy for chemical biology research. J. Am. Chem. Soc. 2022;144:19651–67.

[3] Gollapudi Sunila. Deep learning for computer vision. Learn computer vision using OpenCV. 2019.

[4] Otter Dan, et al. A survey of the usages of deep learning for natural language processing. IEEE Transact Neural Networks Learn Syst 2020;32:604–24.

[5] Orazio Spata Massimo, Battiato Sebastiano, Ortis Alessandro, Rundo Francesco, Calabretta Michele, Pino Carmelo, Messina Angelo. Deep learning algorithm for advanced level-3 inverse-modeling of silicon-carbide power MOSFET devices. Proc. SPIE 12973, workshop on electronics communication engineering (WECE 2023). 2024, 1297309. https://doi.org/10.1117/12.3016130.

[6] Guarnera, Francesco, Alessia Rondinella, Oliver Giudice, Alessandro Ortis, Sebastiano Battiato, Francesco Rundo, Giorgio Fallica, Francesco Traina and Sabrina Conoci. Early detection of hip periprosthetic joint infections through CNN on computed tomography images. In: Foresti, G.L., Fusiello, A., Hancock, E. (eds) Image analysis and processing – iciap 2023. Iciap 2023. Lecture notes in computer science, vol 14234. Springer.

[7] Rondinella Alessia, Crispino Elena, Guarnera Francesco, Giudice Oliver, Ortis Alessandro, Russo Giulia, Lorenzo Clara Di, Maimone Davide, Pappalardo Francesco. Sebastiano Battiato Boosting multiple sclerosis lesion segmentation through attention mechanism. Comput Biol Med 2023;161.

[8] Rundo F, Rinella S, Massimino S, Coco M, Fallica G, Parenti R, Conoci S, Perciavalle V. An innovative deep learning algorithm for drowsiness detection from EEG signal. Computation 2019;7(1):13.

[9] Rundo F, Ortis A, Battiato S, Conoci S. Advanced bo-inspired system for noninvasive cuff-less blood pressure estimation from physiological signal analysis. Computation 2018;6(3):46.

[10] Rundo F, Spampinato C, Conoci S. Ad-hoc shallow neural network to learn hyper filtered photoplethysmographic (PPG) signal for efficient car-driver drowsiness monitoring. Electronics 2019;8(8):890.

[11] Pennisi M, Kavasidis I, Spampinato C, Schinina V, Palazzo S, Salanitri FP, Bellitto G, Rundo F, Aldinucci M, Cristofaro M, Campioni P, Pianura E, Di Stefano F, Petrone A, Albarello F, Ippolito G, Cuzzocrea S, Conoci S. An explainable AI system for automated COVID-19 assessment and lesion categorization from CT-scans. Artif Intell Med 2021;118:102114.

[12] Luo Ruihao, Popp Juergen. Wilhelm Bocklitz Thomas Deep learning for Raman spectroscopy: a review. Analytica 2022;3(3):287–301. https://doi.org/10.3390/analytica3030020.

[13] Dong J, Hong M, Xu Y, Zheng X. A practical convolutional neural network model for discriminating Raman spectra of human and animal blood. J Chemometr 2019;33.

[14] Lee W, Lenferink AT, Otto C, Offerhaus HL. Classifying Raman spectra of extracellular vesicles based on convolutional neural networks for prostate cancer detection. J. Raman Spectrosc. 2019;51(2):293–300.

[15] Kirchberger-Tolstik T, Pradhan P, Vieth M, Grunert P, Popp J, Bocklitz TW, Stallmach A. Towards an interpretable classifier for characterization of endoscopic Mayo scores in ulcerative colitis using Raman spectroscopy. Anal Chem 2020;92:13776–84.

[16] Cheng N, Fu J, Chen D, Chen S, Wang H. An antibody-free liver cancer screening approach based on nanoplasmonics biosensing chips via spectrum-based deep learning. NanoImpact 2021;21:100296.

[17] Fan X, Ming W, Zeng H, Zhang Z, Lu H. Deep learning-based component identification for the Raman spectra of mixtures. Analyst 2019;144(5):1789–98.

[18] Usman Muhammad, Tang Jia-Wei, Li Fen, Lai Jin-Xin, Liu Qing-Hua, Liu Wei, Wang Liang. Recent advances in surface enhanced Raman spectroscopy for bacterial pathogen identifications. J Adv Res 2023;51:91–107. https://doi.org/10.1016/j.jare.2022.11.010. ISSN 2090-1232.

[19] Tang Jiawei, Yuan Quan, Wen Xin-Ru, Usman Muhammad, Yen Tay Alfred Chin, Wang Liang. Label-free surface-enhanced Raman spectroscopy coupled with machine learning algorithms in pathogenic microbial identification: current trends, challenges, and perspectives. Interdiscip. Med. 2024;2(3). https://doi.org/10.1002/INMD.20230060.

[20] Yuan Quan, Yao Lin-Fei, Tang Jia-Wei, Ma Zhang-Wen, Mou Jing-Yi, Wen Xin-Ru, Usman Muhammad, Xiang Wu, Wang Liang. Rapid discrimination and ratio quantification of mixed antibiotics in aqueous solution through integrative analysis of SERS spectra via CNN combined with NN-EN model. J Adv Res 2024. https://doi.org/10.1016/j.jare.2024.03.016. ISSN 2090-1232.

[21] Vildan Dudukcu Hatice, Taskiran Murat, Taskiran Zehra Gülru Çam, Yildirim Tulay. Temporal Convolutional Networks with RNN approach for chaotic time series prediction. Appl Soft Comput 2023;133:109945.

[22] Spata MO, Ortis A, Battiato S, Russo VM. A new deep learning pipeline for acoustic attack on keyboards. In: Arai K, editor. Intelligent systems and applications. IntelliSys 2024. Lecture notes in networks and systems, 1065. Cham: Springer; 2024. https://doi.org/10.1007/978-3-031-66329-1_26.

[23] Zhao Y, Ren J, Zhang B, Wu J, Lyu Y. An explainable attention-based TCN heartbeats classification model for arrhythmia detection. Biomed Signal Process Control 2023;80:104337.

[24] Mikolov Tomas, et al. Recurrent neural network-based language model. Interspeech; 2010.

[25] Massimo Orazio Spata, Rinaudo Salvatore. Virtual machine migration through an intelligent mobile agents system for a cloud grid. Journal of Convergence Information Technology 2011;6:351–60.

[26] Pelletier Charlotte, et al. Temporal convolutional neural network for the classification of satellite image time series. Rem Sens 2018;11:523.

[27] Rizzo Maria Giovanna, Palermo Nicole, Alibrandi Paola, Luigi Sciuto Emanuele, Del Gaudio Costantino, Filardi V, Fazio Barbara, Caccamo Antonella, Oddo Salvatore, Calabrese Giovanna, Conoci Sabrina. Physiologic response evaluation of human foetal osteoblast cells within engineered 3D-printed polylactic acid scaffolds. Biology 2023;12.

[28] Rizzo MG, De Plano LM, Palermo N, Franco D, Nicolò M, Sciuto EL, Calabrese G, Oddo S, Conoci S, Guglielmino SPP. A novel serum-based diagnosis of alzheimer's disease using an advanced phage-based biochip. Adv Sci 2023;10(21):2301650.

[29] Tolstik Tatiana, Marquardt Claudio, Matthäus Christian, Bergner Norbert, Bielecki Christiane, Krafft Christoph, Stallmach Andreas, Popp Jürgen. Discrimination and classification of liver cancer cells and proliferation states by Raman spectroscopic imaging. Analyst 2014;139:22.